

Article

# Vibration Analysis of a 5-DOF Long-Reach Robotic Arm

Hedieh Badkoobehzaveh, Reza Fotouhi \* , Qianwei Zhang and Douglas Bitner

Department of Mechanical Engineering, University of Saskatchewan, Saskatoon, SK S7N 5A9, Canada

\* Correspondence: reza.fotouhi@usask.ca

**Abstract:** In this paper, dynamic and vibration characteristics of a newly developed 5-degrees-of-freedom (5-DOF) long-reach robotic arm for farm applications is studied through finite element analysis (FEA), as well as experimentally. The new manipulator is designed to be light and compact enough that it can be mounted on a small vehicle for farm applications. A finite element model of this novel manipulator was established using a commercial FEA software. FEA was carried out for two different configurations of the manipulator (fully-extended and vertical half-extended). The fully-extended configuration provides the longest reach of the arm and is one of the most commonly used poses in farm applications; vibrations of this configuration are highly affected by its base excitation. The FEA results indicated that the first six natural frequencies of the manipulator for the two configurations considered were between 4.4 to 41.6 (Hz). Modal analysis on the fully-extended configuration was completed using experimental modal analysis to verify the finite element results. In the experiments, acceleration data were obtained utilizing sensors, and were post-processed using Fast-Fourier Transforms. The first six natural frequencies and their corresponding mode shapes were obtained using FEA and also experimentally, and the results were compared; the comparison showed good agreement, with less than 10% difference. Our verified FE model provides a reliable basis for future vibration control for the newly developed robotic arm for different applications. A harmonic response simulation was also carried out using an experimentally corrected FE model; this provides a good understanding of the dynamic behavior of the newly developed arm under base excitation. This paper offers an experimentally corrected FEA model for a large manipulator with base excitation for farm applications.

**Keywords:** vibration of robot manipulator; model corrected finite element analysis; experimental modal analysis



**Citation:** Badkoobehzaveh, H.; Fotouhi, R.; Zhang, Q.; Bitner, D. Vibration Analysis of a 5-DOF Long-Reach Robotic Arm. *Vibration* **2022**, *5*, 585–602. <https://doi.org/10.3390/vibration5030034>

Academic Editors: Kai Zhou, Hongling Ye and Qi Shuai

Received: 30 June 2022

Accepted: 31 August 2022

Published: 3 September 2022

**Publisher's Note:** MDPI stays neutral with regard to jurisdictional claims in published maps and institutional affiliations.



**Copyright:** © 2022 by the authors. Licensee MDPI, Basel, Switzerland. This article is an open access article distributed under the terms and conditions of the Creative Commons Attribution (CC BY) license (<https://creativecommons.org/licenses/by/4.0/>).

## 1. Introduction

### 1.1. Motivation and Background

Vibration analysis and identification are used to investigate dynamic characteristics in a wide range of areas such as biomedical, agricultural, condition monitoring in railway technology [1], and manufacturing. Finite Element (FE) analysis of complex dynamic systems provides an opportunity for building useful computer models to advance research in different aspects of such systems' behavior. High-degree-of-freedom robot manipulators are complex dynamic systems, and vibrations can have adverse effects on both trajectory tracking performance and their stability; the former results in positioning errors and the latter results in damage to actuators and other components and poses safety risks during operation. Multiple research works employed vibration analysis using FEA for robot arms including the works by [2–7]. In [2,3], the researchers performed finite element modal and harmonic analysis on robotic structures to analyze dynamic performance using commercial software. Sahu et al. [4] investigated the effect of cracks in the structure of an industrial robotic arm on vibration by comparing modal analysis results of the robot with and without cracks. Zhou et al. [5] used finite element modal analysis for a robot manipulator in a farming application for its different typical poses with the aim of providing a foundation

for an optimized design. Cheng et al. [6] introduced a planar multi-joint handling robot and investigated the vibration of this robot using finite element modal analysis with SolidWorks. A modal matching analysis of the robot key components was also presented. He et al. [7] used FEA for structural static analysis and modal analysis on a humanoid robot arm. Their results were used for optimum design of the arm. In another research work on humanoid robots, Zhang et al. [8] worked on designing an optimized lightweight structure of a calf structure for a hydraulic biped robot. They performed finite element static and modal analysis on their proposed structure.

In [9], a method was presented for modal analysis and spectrum construction that yielded harmonics and structural modes of vibration. The authors then performed numerical simulations for a 3-DOF system and experimental tests on a 6-DOF flexible manipulator.

In another research work presented in [10], the vibration behavior of a multi-joint flexible robotic arm was analyzed based on obtaining modal parameters using both finite element and experimental methods. Tang et al. [11] performed finite element and experimental modal analysis on a SCARA robot and then attempted to isolate the vibration of the arm by changing the shape of its base to reduce vibration. Liao et al. [12] also established a FE model for the base of a welding robot; finite element modal analysis was conducted for design optimization of the welding robot. Modal experiments along with simulations were also used for assessing vibration reduction efforts for flexible robot links like in [13]. In another study for a biomedical application, Faieghi et al. [14] utilized an empirical approach to study tool vibrations in a robot-driven human glenoid reaming procedure. In [15], experimental modal analysis was used to investigate the effects of non-linearities in joints, different operational poses and the dynamic behavior of a 7-DOF harvesting robot manipulator. In [16,17], the authors presented dynamic models of flexible-joint 6-DOF robot manipulators. They used experimental modal analysis to validate predictions of their dynamic models and the vibration of the manipulators. There are other research works incorporating vibration analysis of robotic manipulators in motion planning or dynamic modeling such as works [18–20].

In [18], vibration analysis was used for a trajectory planning strategy aimed at reducing residual vibration and execution time in industrial manipulators. Min et al. [19] presented a collision detection method and identification scheme for robot manipulators using results from vibration analysis. In [20], the results of a selective modal testing on an industrial robot manipulator were used to identify the stiffness of joints. A dynamic model of the manipulator was also developed. An analytical approach and finite element method were used in [21] to analyze vibration behavior of cable-driven parallel robots. Free vibration results from their methods were compared with results from commercial software. Ivanov et al. [22] performed an analytical study on the problem of protecting a robot arm from small base vibrations. In their research work, they presented a mathematical model for the manipulator motion with small vertical periodic vibrations of the base as well as a model for the vibration isolation of the manipulator. The analytical solution for such a vibration problem incorporated non-linear and complex mathematical equations even for these small base excitations.

In our paper, free (FE and experimental modal analysis) and forced vibration analysis are conducted for a newly-developed 5-DOF long-reach robot manipulator, which is mounted on a moving vehicle traveling on uneven terrain in a farm setting. The problem studied here is somewhat close to the vibration isolation problem presented in [22]; however, base excitation in our application cannot be considered as small vibrations, because farm terrain is rough and produces large amplitude vibrations. In finite element harmonically excited forced vibration analysis, vertical sinusoidal base excitation is numerically modelled. In our work, the aim is to provide useful data for the practical vibration damping of the 5-DOF robot arm and reduce the complexity of the analytical approach to this type of problem.

1.2. The Developed Manipulator

The dynamic system in this study is a 5-DOF hybrid robot manipulator with a compact structure, which has recently been developed and tested as shown in Figures 1 and 2. The main sections of the manipulator are shown; the “upper arm” includes a prismatic upper links and an end-effector. The lower arm includes two parallel links. Detailed kinematics and dynamics analysis of this manipulator is presented in our previous published work in [23]. This manipulator has four rotational joints and one prismatic joint. Constrains for each joint are presented in Table 1. The parallel structure of the manipulator lowers center of gravity of the arm, which reduces the torque requirements for other joints, with the same payload. Each section of the arm’s structure is about one meter long; the prismatic joint provides another one-meter reach, which gives the manipulator a total reach of about three meters. The manipulator is designed to be light (less than 100 kg) and compact enough that it can be fitted onto a small vehicle for farm applications for crop monitoring. These aspects make this manipulator novel, since it is designed to be mounted on a mobile platform. Such a mobile manipulator does not exist commercially [23].

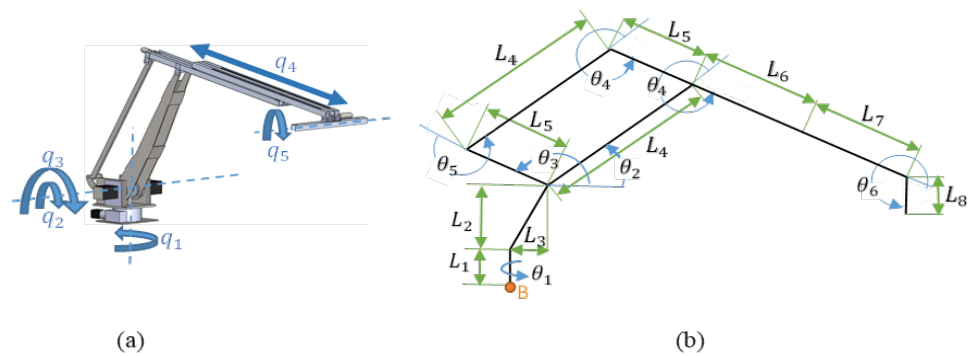


Figure 1. 5-DOF robotic manipulator used here: (a) its DOF; (b) its angles and lengths.

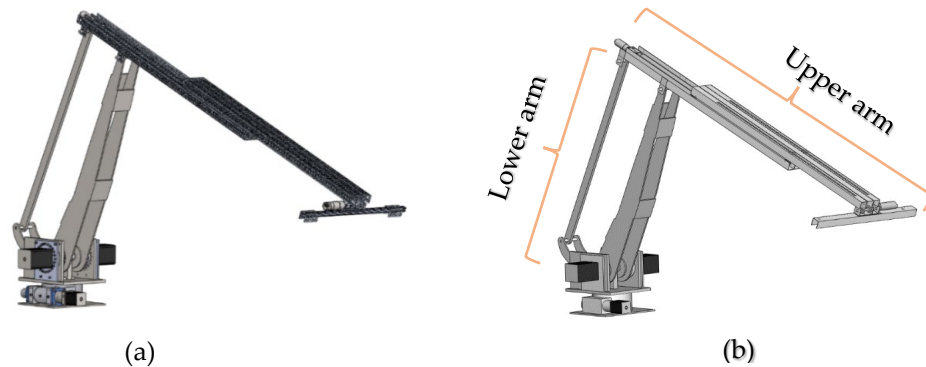


Figure 2. CAD models of the 5-DOF robot manipulator, (a) detailed and (b) simplified.

Table 1. Position Constrains for the manipulator Joints.

Joint	Position Constraints
1	$0^\circ \leq \theta_1 \leq 360^\circ$
2	$0^\circ \leq \theta_2 \leq 120^\circ$
3	$\theta_2 \leq \theta_3 \leq 180^\circ$
4	$0 \leq L_7 \leq 1 \text{ m}$
5	$-90^\circ \leq \theta_6 \leq 90^\circ$

## 2. Finite Element Vibration Analysis

In this section, two types of finite element vibration analysis, including modal analysis and harmonic (forced) analysis are performed to assess the vibration of our 5-DOF robot manipulator; these analyses will shed some light for the future damping of the vibration of this arm.

### 2.1. 3D Model of 5-DOF Robot Manipulator

Our system is a 5-DOF robot manipulator. For complex geometry models, it is necessary to simplify the models for finite element analysis. The key point is to ignore geometry complexities, which have minor effects on results of specific analysis of interest. A simplified model of the robotic manipulator was used with the following simplifications and assumptions:

1. To prevent meshing complications, most bolts, nuts and bearings were removed and some parts (motors, gear box and upper link) were replaced with similar simpler geometries having similar masses by removing tiny features such as fillets and screw threads, or removing holes and reducing the thickness of beams to compensate for the added mass.
2. Deflections are assumed to be small. This assumption is verified by finite element and experimentally; the manipulator's tip deflection compared with its overall length are small based on Euler-Bernoulli beam theory.
3. The system is assumed to be linear for modal analysis. The vibration of the manipulator in the fully extended-configuration is similar to the vibration of a cantilever beam with small deflections. This means that the ratio of tip deflection over length of cantilever is less than 10%, and Euler-Bernoulli beam theory is valid in this case; superpositions can also be used for this system, as for linear systems.

Detailed and simplified models of the robot manipulator are shown in Figure 2. The geometry of the robot manipulator in the present paper is divided into two main areas named "lower arm" and "upper arm" to discuss the effects of vibration. The "upper arm" includes the linear actuator, the extension upper links and the end-effector. The lower arm includes the parallel lower links.

### 2.2. Modal Analysis Process

The 3D simplified CAD model of the manipulator for two configurations of the robot structure were created using SOLIDWORKS (2020 SP3.0 Education Edition, SolidWorks Corp., Waltham, MA, USA) and were imported to ANSYS (2021 Edition, Ansys, Inc., Canonsburg, PA, USA), a commercial finite element analysis software package [24]. Two different configurations of the robot structure, which are the two that will most probably be used in the field, were chosen as the targeted geometries in modal analysis (shown in Figure 3). Structural steel was assigned to most parts in the lower arm area of the manipulator and for the upper area, the material was mostly aluminum alloy. All automatically defined connections were manually checked and corrected to achieve the highest possible accuracy. The next step was mesh generation. Here, "Automatic" grid division and the sizing function of "Adaptive" with different element sizes ranging from 7 mm to 20 mm were defined to prevent bodies with one element pass through the thickness, while obtaining a high-quality mesh. The fully-extended configuration (Figure 3a) structure was divided into 60,565 elements and 227,493 nodes; the half-extended configuration (Figure 3b) was divided into 60,593 elements and 227,768 nodes. The meshed structure for the fully-extended configuration is also shown in Figure 4. Due to the different number of elements produced by the automatic method in each configuration, the total number of elements and nodes are different for the two configurations. The fixed support was used as a boundary condition for modal analysis, as shown in Figure 5.



Figure 3. CAD model for (a) Fully-extended Configuration, (b) Vertical Half-extended Configuration.

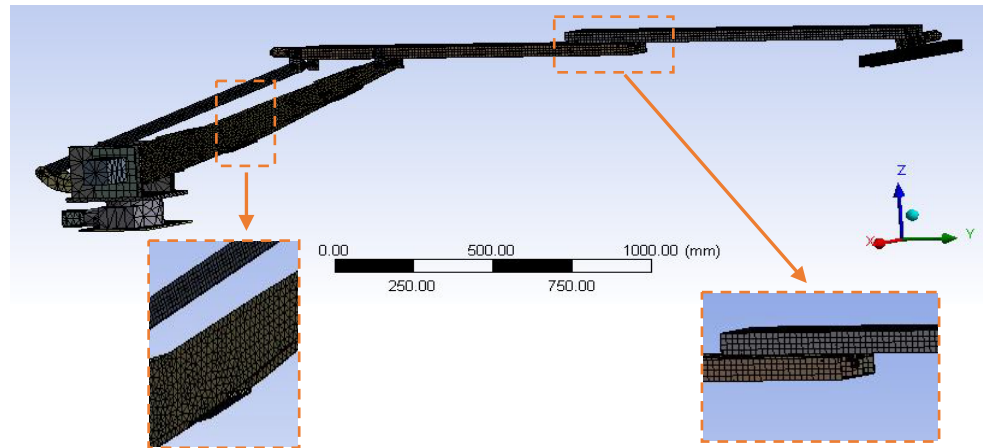


Figure 4. Fully-extended Configuration meshed structure.

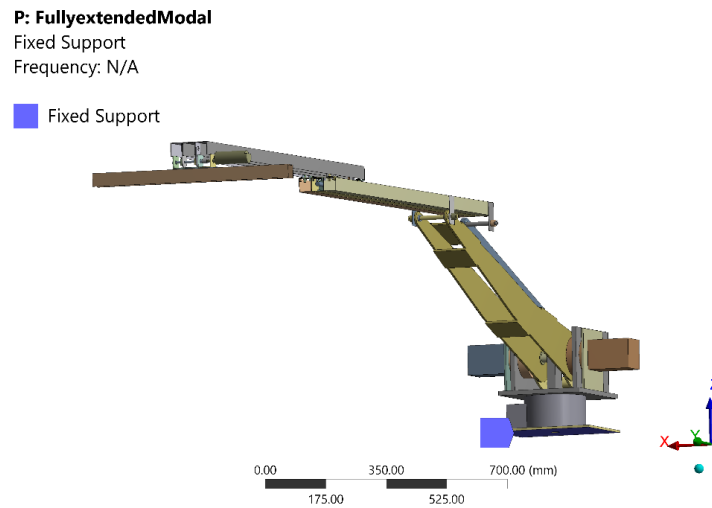


Figure 5. Fixed support is used for modal analysis of the fully extended configuration.

### 2.3. Modal Analysis Results

The first six natural frequencies and their corresponding mode shapes were obtained using modal analysis for both configurations. Our 5-DOF robot manipulator was developed for a farm/crop breeding setting with rough terrain. The intended application is crop monitoring for plants such as canola and wheat. The manipulator with some sensors attached to its end-effector is designed for a moving vehicle such as a tractor or unmanned ground vehicle traveling roads that collects data from targeted crops for phenotyping (monitoring traits of crops). The frequency range of ground excitation induced to the manipulator base was measured in field tests. This real base excitation frequency range is important for forced vibration analysis and vibration control of the manipulator. The dominant measured excitation frequencies were closer to the lower natural frequencies

obtained using finite element analysis. By gathering the first six natural frequencies and their corresponding mode shapes, we will have sufficient results and there will be no need to consider higher frequencies for our farm application. The first six natural frequencies for the two configurations are presented in Tables 2 and 3. The first six corresponding mode shapes for the fully-extended configuration are demonstrated in Figures 6–11. Each mode shape is shown from two different views to demonstrate 3D movement. Figures 6 and 7 show the total deformation of the arm when the first and the second mode shapes are excited, dominated mostly by the upper arm lateral motion. Figures 8 and 9 show deformation for the third and the fourth modes; maximum deformation occurs at both ends of the upper arm due to torsional vibration. Figures 10 and 11 show the deformation for the fifth and the sixth modes, when bending dominates; this results in deformation at the middle of the upper and lower arm where maximum bending occurs. Figure 12 shows location of base excitation of the fully-extended robot configuration for harmonic analysis. Similar observations are true for Figures 13–18, which come later.

**Table 2.** Natural frequencies of the fully-extended configuration.

Mode	Frequency [Hz]
1.	4.83
2.	7.10
3.	12.25
4.	18.84
5.	29.91
6.	41.63

**Table 3.** Natural frequencies of the half-extended configuration.

Mode	Frequency [Hz]
1.	5.21
2.	7.16
3.	14.86
4.	18.12
5.	33.49
6.	38.82

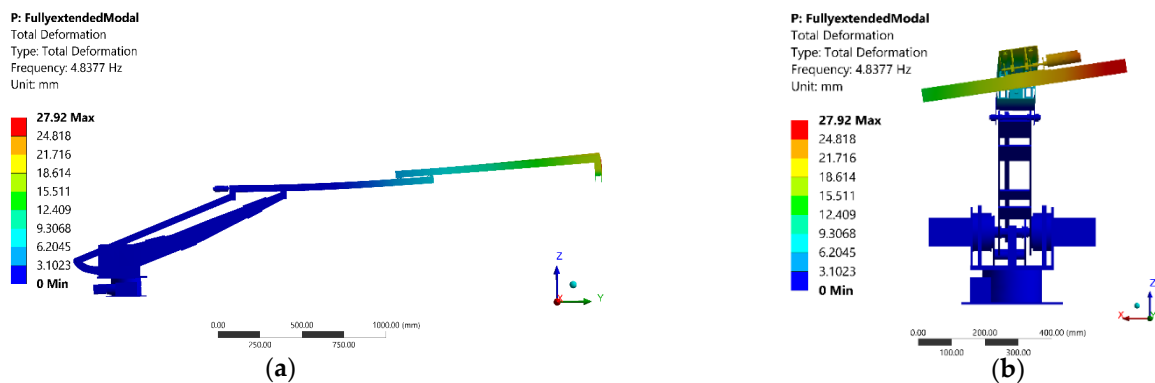


**Figure 6.** The 1st mode shape of vibration for the Fully-extended configuration, arm is fixed at the base (a) side view & (b) front view.

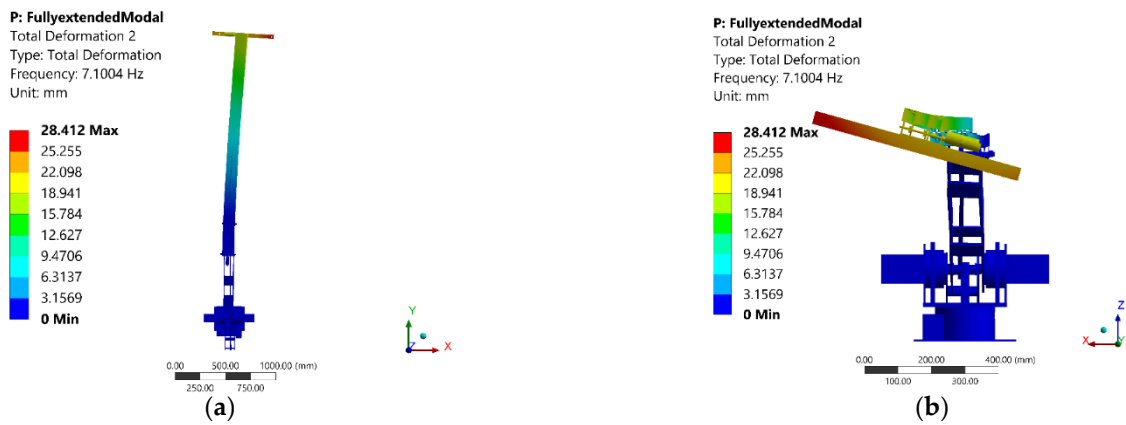


Figure 7. The 2nd mode shape of vibration for the Fully-extended configuration, arm is fixed at the base (a) top view & (b) front view.

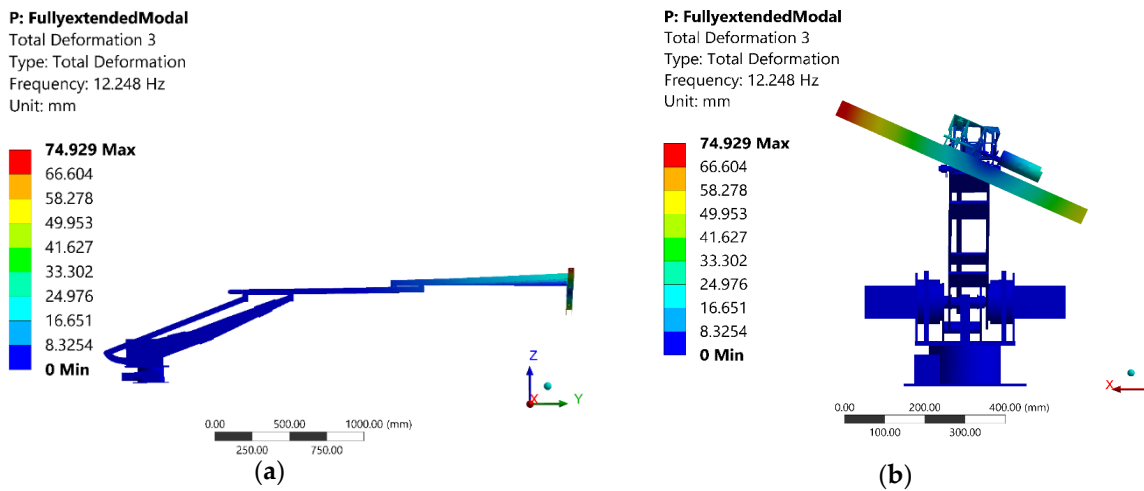


Figure 8. The 3rd mode shape of vibration for the Fully-extended configuration, arm is fixed at the base, (a) side view & (b) front view.

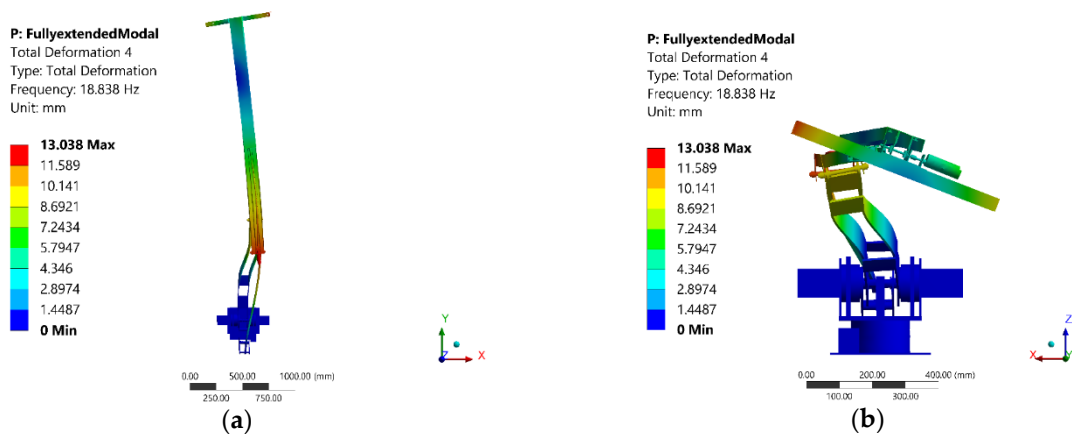


Figure 9. The 4th mode shape of vibration for the Fully-extended configuration, arm is fixed at the base (a) top view & (b) front view.

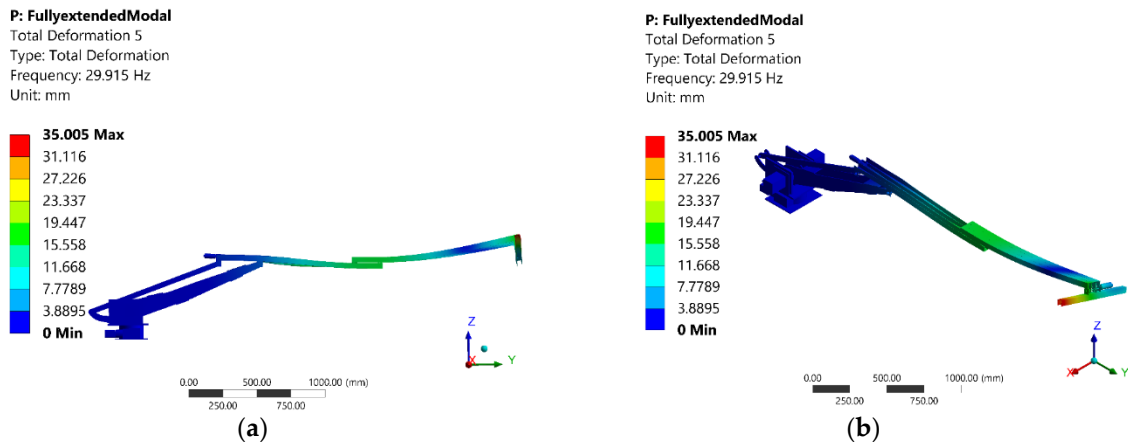


Figure 10. The 5th mode shape of vibration for the Fully-extended configuration, arm is fixed at the base (a) side view & (b) isometric view.

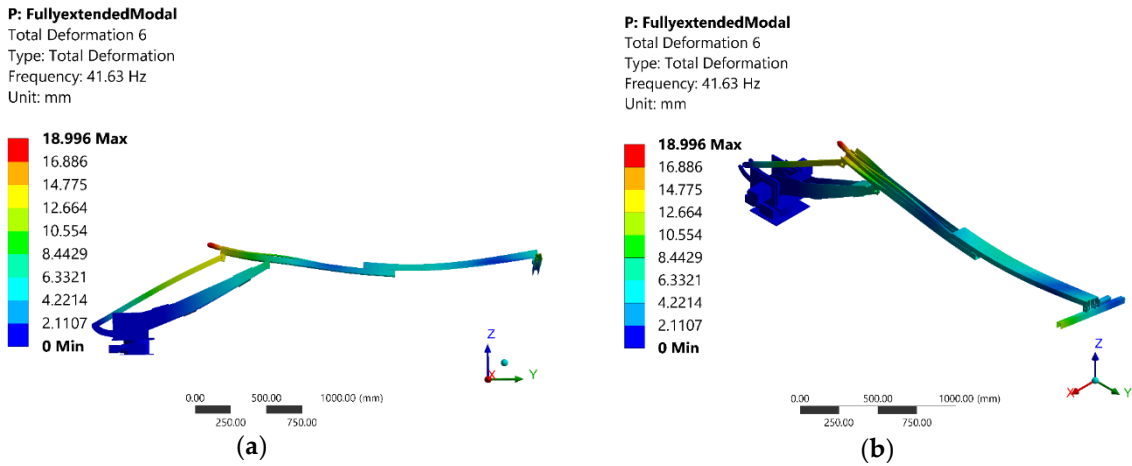


Figure 11. The 6th mode shape of vibration for the Fully-extended configuration, arm is fixed at the base (a) side view & (b) isometric view.

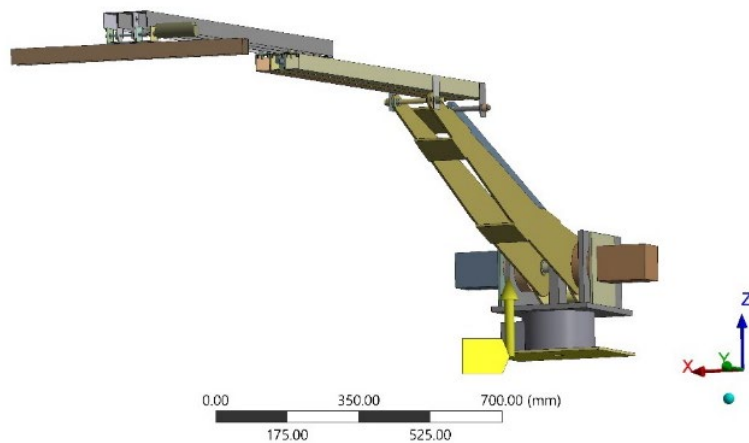
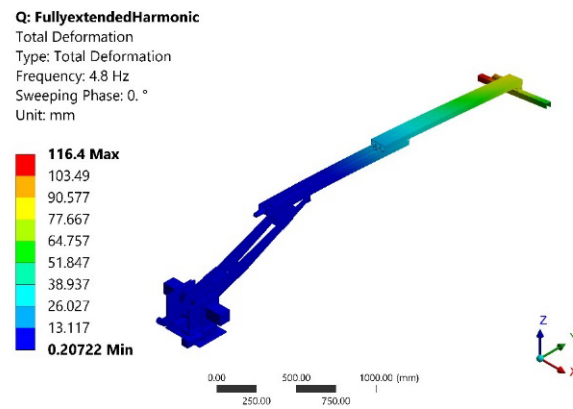
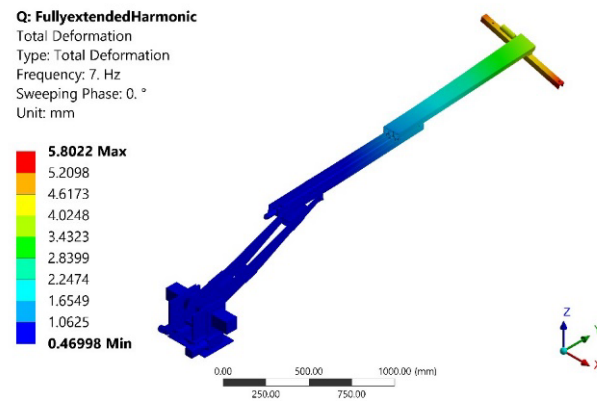


Figure 12. Harmonic analysis, base excitation is applied in upward Z-direction to the base of robot.



**Figure 13.** Total deformation (in mm) of the fully-extended configuration of the manipulator, resulting from the harmonic analysis at the first natural frequency (4.8 Hz).



**Figure 14.** Total deformation (in mm) of the fully-extended configuration structure resulting from the harmonic analysis at the 2nd natural frequency (7 Hz).

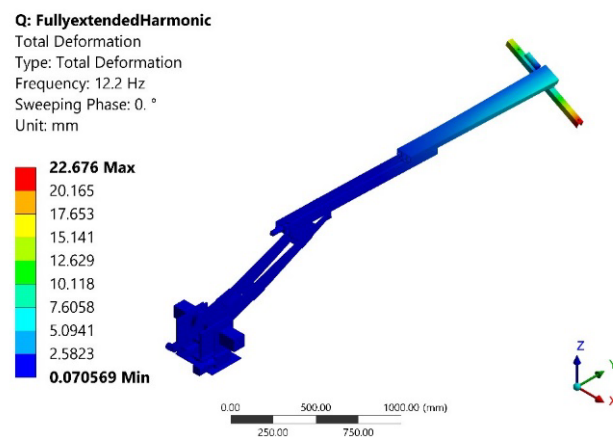


**Figure 15.** Total deformation (in mm) of the fully-extended configuration structure resulting from the harmonic analysis at the 3rd natural frequency (12.2 Hz).

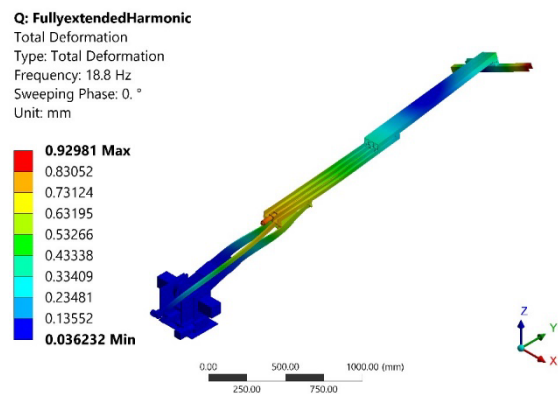


**Figure 16.** Total deformation (in mm) of the fully-extended configuration structure resulting from the harmonic analysis at the 4th natural frequency (18.8 Hz).

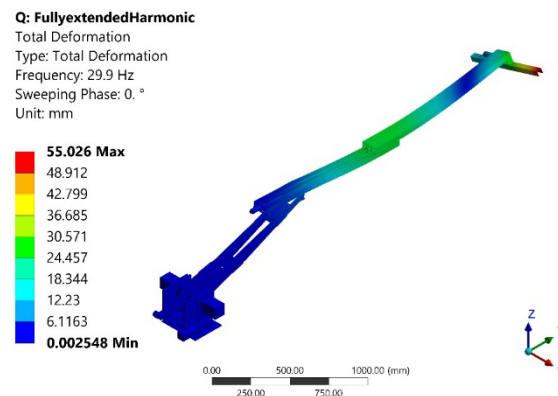


**Figure 17.** Total deformation (in mm) of the fully-extended configuration structure resulting from the harmonic analysis at the 5th natural frequency (29.9 Hz).

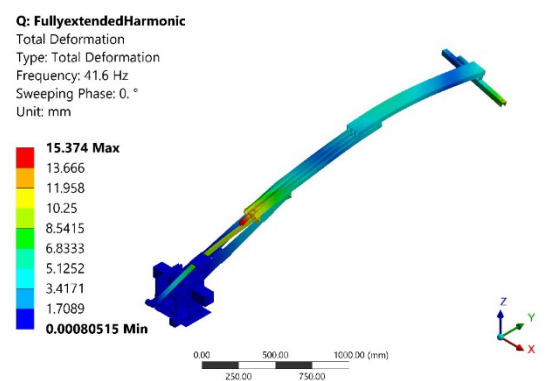


**Figure 18.** Total deformation (in mm) of the fully-extended configuration structure resulting from the harmonic analysis at the 6th natural frequency (41.6 Hz).

The maximum displacement shown on the mode shape figures using FEA in the modal analysis is not a real value (as no specific loading input is defined in the simulation). This could be used as a relative value between different parts of the model as well as an indicator for the most affected parts of the model.

#### 2.4. Harmonic (Force) Vibration Analysis Process

In a harmonic response analysis, steady response of the system with sinusoidal varying input force is determined. The excitation function is a sine function with constant amplitude [2].

A harmonic forced response simulation was also carried out using our experimentally corrected FE model and based on the results obtained from the experimentally verified modal analysis; this provides a good understanding of the dynamic behavior of the newly developed arm under base excitation.

In this part, FEA for harmonically excited base motion for the fully-extended configuration model of the robot manipulator is presented. External base excitation is present in the farm application considered. It is of great significance to investigate this situation for the investigation of the damping of vibrations. This type of analysis was carried out with the aim of finding the effects of harmonic excitation on the structure. This type of analysis uses a mode-superposition method. The first step for this analysis is modal analysis. Next, the modal results are transferred to the harmonic analysis and a frequency response of the system to the applied harmonic excitation is obtained. For our specific application, the base excitation induced from the moving vehicle traveling on the uneven terrain would not be an accurate harmonic excitation; however, it could be estimated as harmonic excitation with simplification. The input base excitation frequency range was defined as between 1 to 50 Hz, which covers the range of the first six natural frequencies in modal analysis; this frequency range includes specific values close to the first six natural frequencies to simulate semi-resonance situations. Several vibration tests were carried out in a target field to estimate the average excitation acceleration amplitudes transferred to the base of the robot manipulator. Based on the average measured vertical acceleration at the manipulator's base during field tests, the amplitude of  $1 \text{ m/s}^2$  was selected; this value is a good approximation to the real maximum excitation at the base and can be used for the simulated harmonic analysis; also, acceleration data from the IMU attached to the base at the field trials, confirm our selection. As shown in Figure 12, input excitation is applied to the base of the fully-extended robot configuration; this excitation comes from the moving vehicle. This is the boundary condition that is applied instead of the fixed support considered in the modal analysis.

### 2.5. Harmonic (Force) Vibration Analysis Results

The first six natural frequencies of the fully-extended configuration of the robot are given in Table 2; these values were used for the harmonic analysis. The total deformation of the fully-extended configuration of the arm at the first six natural frequencies, obtained from harmonic analysis, are shown in Figures 13–18; a summary of these results is given in Table 4. The frequency responses of the end-effector deformation in three different directions resulting from the harmonic analysis are shown in Figure 19. For this harmonic analysis, external base excitation was a sinusoidal acceleration with frequencies close to the natural frequencies. The results for this analysis will be discussed further in Section 4.

**Table 4.** Harmonic (forced) analysis results, maximum total deformation values and their locations at the fully-extended configuration; external base excitation was a sinusoidal acceleration with frequencies close to the natural frequencies.

Mode	Frequency [Hz]	Deformation Value (mm)	Deformation Location
1	4.83	116.4	End-effector
2	7.10	5.802	End-effector
3	12.25	22.68	End-effector
4	18.84	0.929	End-effector & Joint 4
5	29.91	55.03	End-effector
6	41.63	15.37	Joint 4

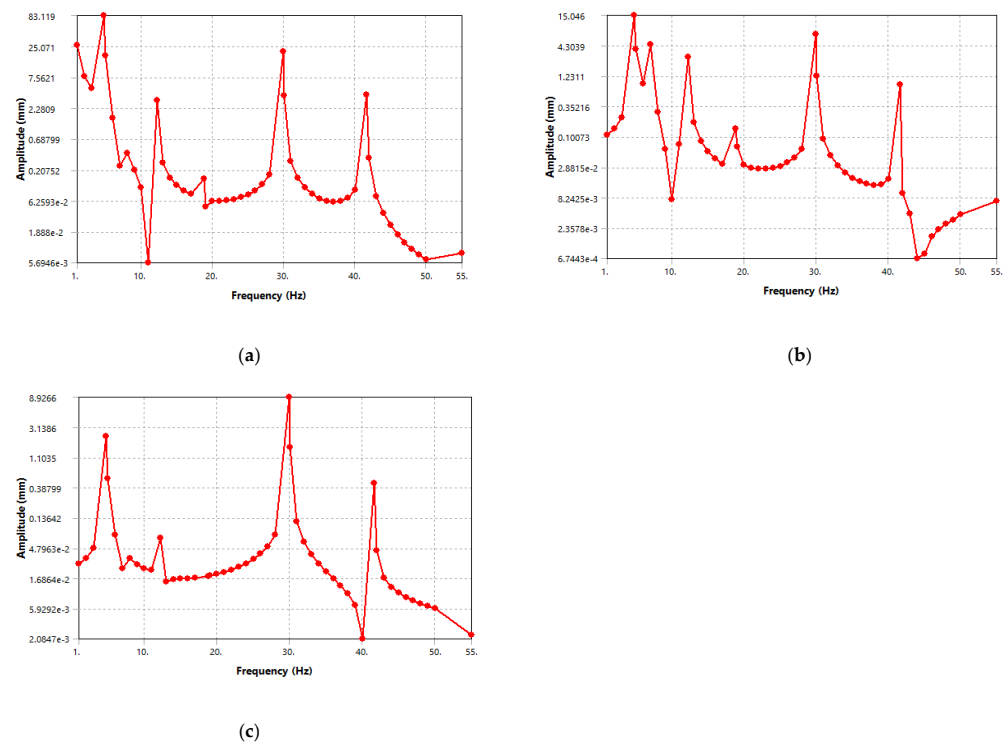


**Figure 19.** Frequency response of the harmonic analysis for the end-effector deformation in vertical (a), lateral (b) and axial (c) directions. External base excitation were sinusoidal accelerations with frequencies close to the natural frequencies, as listed in Table 4.

### 3. Experimental Modal Analysis and Results

This section covers an experimental modal analysis test performed on our 5-DOF manipulator. In a laboratory setting, the fully-extended manipulator configuration (see Figure 20a) was excited by a hammer, as shown in Figure 20b, while three accelerometers, one Inertial Measurement Unit (IMU) and one Vertical Reference Unit (VRU) were used to measure the vibration response of the manipulator. IMU (MTi 630 IMU from XSSENS) and VRU (3DM-GX5-15 VRU from LORD SENSING Microstrain) sensors with integrated accelerometers, measured accelerations (in x, y and z directions) of the manipulator at the end-effector and at the middle of the upper arm; three single-axis accelerometers, which were attached to the manipulator in the three different directions of x, y and z (shown in Figure 21) also measured accelerations at the same locations.

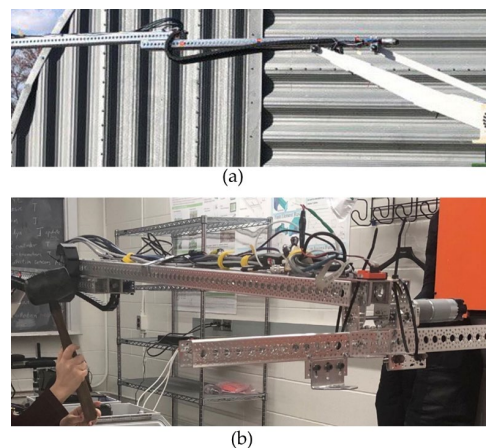


**Figure 20.** (a) the 5-DOF manipulator at fully-extended configuration, (b) hammer test to the fully-extended manipulator for experimental modal analysis.

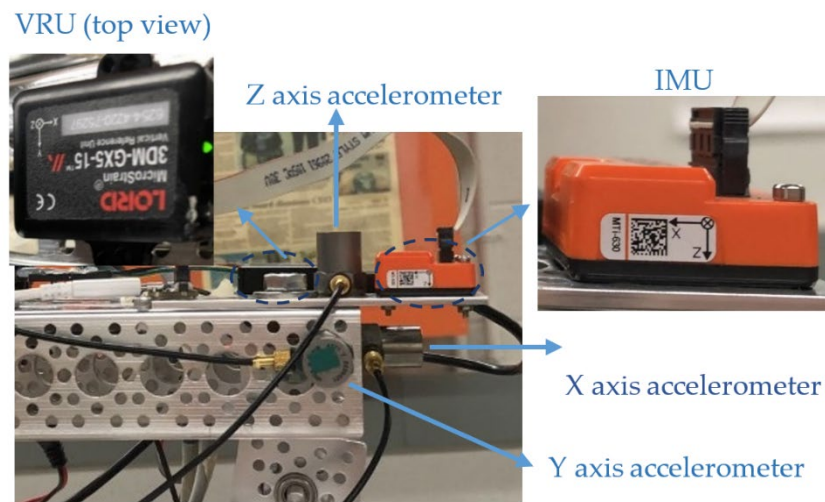


**Figure 21.** Experimental Modal analysis setup, locations of accelerometers, IMU and VRU sensors attached to the manipulator top-link end-point.

A few different test scenarios were carried out to optimize the location of sensors, excitation location (hammer’s impact to the arm) on the manipulator, and the direction of excitation. The obtained results from the sensors were analyzed to obtain the arm’s natural frequencies. A Fast Fourier Transform (FFT) was used to convert acceleration results from the time-domain to the frequency domain.

The results of the sensors were compared, and high and isolated peaks of the frequency response plots for different tests were obtained as the experimental natural frequencies. Accelerometers were calibrated and verified for their accuracy. The natural frequencies obtained from the VRU and from the accelerometers showed a very good agreement. The obtained data from the IMU with its set sampling frequency (400 Hz) showed less accuracy in capturing lower natural frequencies (under 12 Hz) compared to the other sensors used.

The VRU unit data acquisition was set with a sampling frequency of 1000 Hz and 25,804 samples (19,347 samples in some tests). A sample of the experimental modal response of the fully-extended manipulator resulting from FFT analysis on the accelerometers data and the VRU data are shown in Figure 22. In this Figure, X represents frequency value, and Y represents relative magnitude from FFT (Fast Fourier Transform) analysis. This Figure shows only the first six natural frequencies for the manipulator in the given configuration. More discussion is given in the discussion section.

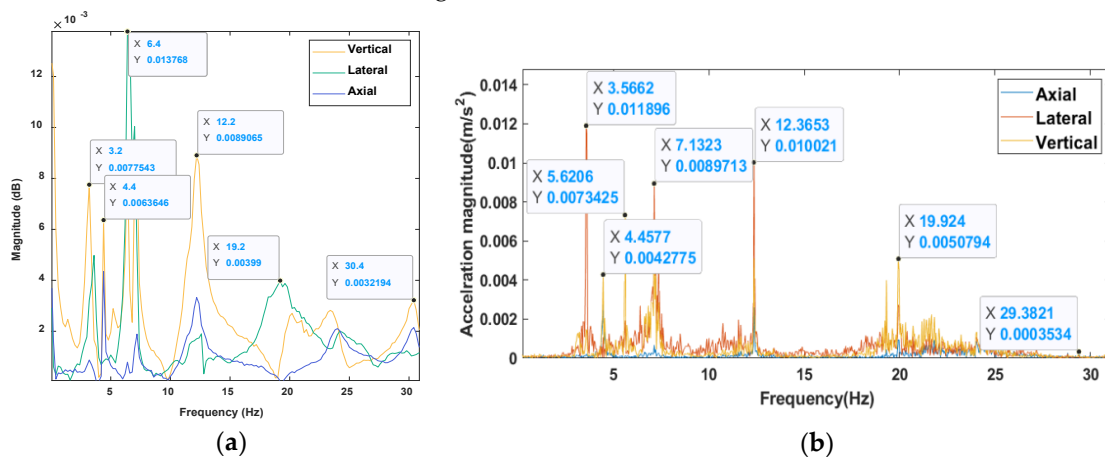


**Figure 22.** Experimental results, natural frequency response of the fully-extended manipulator under axial excitation at the end-effector obtained from (a) accelerometers data and (b) the VRU data.

There are other Frequency Response Function (FRF) plots from more experiments that are in very good agreement for lower frequencies and some captured higher frequencies as well. The average values of peak points of the plots are concluded as experimental natural frequencies and are presented in Table 5.

**Table 5.** Comparison of Natural Frequencies Obtained from Experimental and Finite Element Analysis.

Mode	Experimental (Hz)	FEA (Hz)	Percentage Difference
1'	3.1–3.56	3.2	~4%
1	4.4	4.8	~9%
2'	5–5.6	5.5	~3.7%
2	6.4–7.2	7.1	~4.4%
3	11.9–12.4	12.2	~0.4%
4	18.6–21	18.8	~5%
5	24–31.5	29.9	~7.7%
6	38–43.2	41.6	~2.5%

#### 4. Discussion

The following sub-sections are a discussion of the finite element and experimental results presented in Sections 2 and 3.

##### 4.1. Comparison of Experimental and Finite Element Modal Analysis Results

In this section, the experimental and finite element modal analysis results are compared and the difference between them is discussed for the fully-extended configuration.

Table 5 indicates a comparison of results obtained for natural frequencies. The second column in Table 5 shows the range of peak values of the FRF results gathered from all different modal experiments; the third column of Table 5 presents natural frequency values resulting from FEA corresponding to each mode of vibration indicated in the first column. In the experimental tests performed, the robotic arm was attached to a mounting structure and was placed on a table without completely fixing its base (see Figure 23). The structure and boundary condition for the experimental tests were not exactly the same as the analysis in Section 2. Another issue of this comparison is the possibility of loose bolts, which makes the actual manipulator less stiff than the simulated one. To model a loose connection in FEA, the “normal stiffness” value of that contact was lowered. As a result, the modal analysis result on the modified model showed the first natural frequency to be about 3.2 Hz in comparison with the experimental frequency of 3.1–3.56 Hz; this frequency was not obtained from the previous model. This shows that loose bolts can be a source of error if not completely fixed.

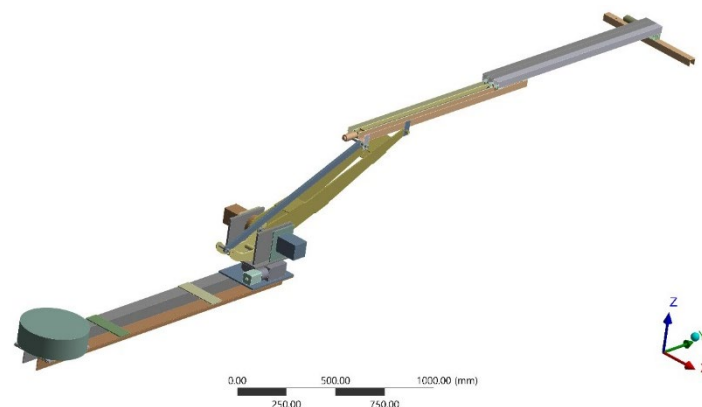


**Figure 23.** CAD Model for modified FEA setup for the fully-extended manipulator.

The FEA model was later modified to be closer to the actual manipulator setup as shown in Figure 23. The FEA results then produced modes 1' and 2' in Table 5. Here, the overall experimental and FEA natural frequency results match well with each other (less than 10% differences); the natural frequency values with a fixed support boundary condition at the base are given as modes numbered 1 to 6 in Table 5. The percentage difference between the average experimental natural frequency and FEA natural frequency values for each mode is presented in the 4th column of Table 5. To see the corresponding mode shapes for each mode, see Figures 6–11.

Simplifications made on the 3D model of the manipulator resulted in a slightly different total mass of the structure and slightly different connections, meaning a different stiffness for the arm; such simplifications as well as not enough high-quality mesh would be sources of errors from the finite element analysis. The backlash, loose mechanical connections, unfixed electrical wires in the assembled structure of real arm as well as sensor accuracy limitations and noise would also be sources of errors from the experiments.

#### *4.2. Discussion of Mode Shapes and Effect of Different Configurations of the Manipulator on the Modal Analysis Results*

As the FEA results indicate, the first and the second mode shapes (Figures 6 and 7) are mostly dominated by the vertical and lateral movement of the upper arm, respectively. In both of these modes, a little rotational movement of the upper arm around its longitudinal axis is present; this is mostly from the end point of the upper arm, due to having an electrical motor at one side of the end-effector.

The mode shapes related to the third and the fourth natural frequencies are mostly dominated by the torsional vibration; the former shows torsional movement mostly by the upper arm and the latter includes torsional movement of both the upper and lower arm areas.

Mode shapes 5 and 6 indicate bending movement as the dominant vibration mode. The 5th mode shows bending movement mainly by the upper arm area while in the 6th mode, some bending movement contribution from the lower arm is also added to the bending of the upper arm area.

As is evident from Figures 6–11, the upper arm area is mostly prone to vibration and deformation (especially in the fully-extended configuration); this could be predicted due to the high length to width ratio of the upper arm (which is like a long slender beam) and its material (aluminum alloy) which is less stiff than the structural steel used for the lower arm area.

The overall natural frequency values for the vertical half-extended configuration (see Table 3) are higher than the fully-extended configuration indicating higher overall stiffness of that configuration. This was predictable as this configuration has a more compact structure. The dominant movement of the mode shapes corresponding to the first two natural frequencies of the vertical half-extended configuration are the opposite of the ones for the fully-extended configuration. This shift in the mode shapes is associated with different overall stiffness along different axes of the robotic manipulator structure. Reducing the length of the upper arm and moving the lower arm upward in the vertical half-extended configuration changes the overall stiffness of the structure and its center of mass location. In this case, the lateral movement of such a configuration needs less energy to be completed than the vertical displacement. The other mode shapes of the two configurations show almost the same type of dominant movement with small differences such as in the 6th mode of the half-extended configuration, where torsional movement is present.

#### *4.3. Harmonic (Force) Response Discussion*

The results presented for the harmonic analysis show the dynamic response of the manipulator to a user-defined external base excitation in the form of sinusoidal acceleration. The input excitation frequencies were chosen intentionally to be close to the first six natural frequencies of the manipulator to demonstrate the worst-case scenarios for vibration.

From Figures 13–18, total deformation of the arm, when the first and the second mode shapes are excited, it is mostly dominated by the upper arm due to the lateral motion of the upper arm. For the third and the fourth modes, maximum deformation occurs at both ends of the upper arm due to torsional vibration. For the fifth and the sixth modes, bending dominates, which results in maximum deformation at the middle of the upper and lower arm, where maximum bending occurs.

The total deformation distribution of the fully-extended manipulator at the first six natural frequencies (Figures 13–18) confirms that intense oscillations occur at the end-effector. It would be of great significance to study the deformation and vibration of the end-effector, since the end-effector holds the monitoring sensors in the farm application and its vibration directly affects the data-collection accuracy. The frequency-response for the deformation of the end-effector in the vertical, lateral and axial directions were studied. The high vibration amplitude values when the excitation frequency becomes close to one of the natural frequencies (resonance) can be seen in the frequency responses (Figure 19). Based on the simulated results obtained for  $1 \text{ m/s}^2$  amplitude of base excitation, the maximum deformation of the end-effector in the vertical ( $z$ -axis), lateral ( $x$ -axis), and axial ( $y$ -axis) directions were 83.1 mm at 4.8 Hz input frequency, 15 mm at 4.8 Hz input frequency and 8.9 mm at 29.9 Hz input frequency, respectively. The end-effector deforms mostly in the vertical direction, which is predictable, as the first mode shape showed dominant vertical movement and the base excitation was also applied in the vertical direction. The numerical results for the selected excitation give a good understanding of the deformation scales for different parts of the structure. However, in real resonance situations, with closer excitation frequencies to the natural frequencies, even higher amplitudes of vibration could have resulted.

## 5. Conclusions

In this study, vibration behavior of a newly developed 5-DOF robot manipulator for free and forced excitation was investigated. The dominant natural frequencies of the new manipulator were obtained numerically for two typical configurations of the manipulator, which are prone to vibration during operation. The results indicated that the first six natural frequencies of the manipulator for the two configurations considered were between 4.4 to 41.6 (Hz). A comparison of the natural frequencies for the two configurations showed different values, which was predictable due to different mass distributions and different stiffness. As known, more stiff structures result in higher natural frequencies. Based on the FEA results, the first two modes of vibration are mostly dominated by the vertical and lateral motion of the upper arm. It was found that the upper arm of the manipulator is more prone to vibration; this is especially true for the fully-extended configuration, due to the high length to width ratio of the upper arm, and due to its less stiff material (aluminum alloy) compared with the more stiff material of the lower arm (structural steel).

The vibration analysis for the fully-extended manipulator, which is highly affected by its base excitation, was studied using experimental modal analysis and FEA harmonic (force) analysis. The FEA and experimental modal analysis results matched well, with less than 10% difference. The verified finite element model of the manipulator and the results obtained from modal analysis can be used in the vibration control of such a manipulator. For this purpose, the mode shapes (eigenvectors) can be used to build state-space models of the manipulator and a control strategy to control and/or damp vibration at specific nodes (e.g., nodes located at the joints). Using such a reliable FEA eliminates the need for a complex analytical vibration control analysis for this manipulator. The work presented in [22] dealt with the problem of vibration protection of a manipulator with small vibrations induced from its base. In that study, closed-form mathematical models were used for describing motion of the manipulator; small vibrations of the manipulator were described using a second-order nonlinear differential equation. Although the topic of the research discussed here is close to the vibration isolation presented in [22], the issue is solved using a different analysis, which included finite element analysis combined with experimental

verification. Also, the base excitation in a farm application is not necessarily small, thus complex mathematical equations should be used for an analytical solution. The system studied in this paper is a newly developed robot manipulator, thus the vibration behavior needs to be studied; no similar study has been presented in other published works for such a large manipulator.

The harmonic analysis results showed that the base harmonic excitation could result in significant vibration at the end-effector of the manipulator. Numerical results of this analysis for different amplitudes of excitation gave a good indication of what a safe range for the excitation frequency is for operation of this manipulator. The results presented are encouraging for the active vibration control of such manipulators with base excitation. This vibration analysis can also be extended to more complex forced vibration analysis, such as transient vibration analysis using experimentally measured base excitation, and for different applications. This paper offers an experimentally corrected FEA model for a large manipulator with base excitation for farm applications. The vibration analysis presented here can be improved by considering joint damping (friction) to obtain a more accurate FEA model, which would be closer to an actual manipulator.

**Author Contributions:** H.B.: planned and carried out vibration analysis simulations; planned and executed experiments; analyzed experimental and simulation results; prepared the manuscript. R.F.: supervised this research, provided funding, advised on experimental tests and simulation analysis; provided extensive technical and editorial comments and edited the manuscript. Q.Z.: contributed to the analysis of experimental results by providing a code for analyzing the results of accelerometers; provided technical and editorial comments on the manuscript. D.B.: contributed to the experimental analysis; advised on analysis of experimental data; provided technical and editorial comments on the manuscript. All authors have read and agreed to the published version of the manuscript.

**Funding:** This work was supported by a Canada First Research Excellence Fund (CFREF) through the Global Institute for Food Security (GIFS), University of Saskatchewan, Canada. Also, funding was provided by an NSERC-CRD grant no. 514648-17 of Reza Fotouhi, and an industrial partner.

**Acknowledgments:** This research was conducted in the Robotics Lab at the University of Saskatchewan. The role of other lab members, especially, Amir Mohamad Kamalirad, Joshua Cote, Mohammad Amir Khozeimeh, Majid KhakPour is gratefully acknowledged. The authors wish to acknowledge the College of Agriculture and Bioresources, especially, Pierre Hucl and Michael Grieman.

**Conflicts of Interest:** The authors declare no conflict of interest.

## References

1. Soto-Ocampo, C.R.; Mera, J.M.; Cano-Moreno, J.D.; Garcia-Bernardo, J.L. Low-Cost, High-Frequency, Data Acquisition System for Condition Monitoring of Rotating Machinery through Vibration Analysis-Case Study. *Sensors* **2020**, *20*, 3493. [[CrossRef](#)] [[PubMed](#)]
2. Tang, Y.; Yu, Y.; Shi, J.; Zhang, S. Modal and harmonic response analysis of key components of robotic arm based on ANSYS. *Vibroengineering Procedia* **2016**, *12*, 109–114.
3. Udameeshi, S.; Patil, G.S.; Patil, M.V. Finite element analysis of pick and place robotic structure. *Int. Res. J. Eng. Technol.* **2017**, *3*, 1497–1500.
4. Sahu, S.; Choudhury, B.B.; Biswal, B.B. A vibration analysis of a 6 axis industrial robot using FEA. *Mater. Today Proc.* **2017**, *4*, 2403–2410. [[CrossRef](#)]
5. Zhou, J.; Yang, Z.; Chen, S. Analysis of the harvesting robot arm modal based on CAE. *J. Chem. Pharm. Res.* **2014**, *6*, 669–673.
6. Cheng, L.; Wang, H. Finite element modal analysis of the FPD glass substrates handling robot. In Proceedings of the 2012 IEEE International Conference on Mechatronics and Automation, Chengdu, China, 5–8 August 2012; IEEE: Piscataway, NJ, USA, 2012. paper no. 6284331. pp. 1341–1346.
7. He, D.T.; Guo, Y. Finite element analysis of humanoid robot arm. In Proceedings of the 2016 13th International Conference on Ubiquitous Robots and Ambient Intelligence (URAI), Xi'an, China, 19–22 August 2016; IEEE: Piscataway, NJ, USA, 2016; pp. 772–776.
8. Zhang, J.; Yuan, Z.; Yuan, W.; Dong, S. Lightweight Design and Modal Analysis of Calf Structure of Hydraulic Biped Robot. In Proceedings of the 2020 10th Institute of Electrical and Electronics Engineers International Conference on Cyber Technology in Automation, Control, and Intelligent Systems (CYBER), Xi'an, China, 10–13 October 2020; IEEE: Piscataway, NJ, USA, 2020; pp. 146–151.

9. Vu, V.H.; Liu, Z.; Thomas, M.; Hazel, B. Modal analysis of a light-weight robot with a rotating tool installed at the end effector. *Proc. Inst. Mech. Eng. Part C J. Mech. Eng. Sci.* **2017**, *231*, 1664–1676. [[CrossRef](#)]
10. Liu, Z.; Song, L.B.; Li, Y.; Pan, B.Z. Comparison of finite element and experimental modal analysis of multi-joint flexible robotic arm. In Proceedings of the 2017 International Conference on Mechanical, System and Control Engineering (ICMSC), St. Petersburg, Russia, 19–21 May 2017; IEEE: Piscataway, NJ, USA, 2017. paper no. 2021, 7959450. pp. 96–100.
11. Tang, Z.; Pan, Y.; Cheng, Z. Vibration analysis and passive control of SCARA robot arm. In Proceedings of the 2019 International Conference on Robotics, Intelligent Control and Artificial Intelligence, Shanghai, China, 20–22 September 2019; Association for Computing Machinery: New York, NY, USA, 2019; pp. 89–93.
12. Liao, X.; Gong, C.; Lin, Y.; Wang, W. The finite element modal analysis of the base of welding robot. In Proceedings of the 2010 3rd International Conference on Advanced Computer Theory and Engineering (ICACTE), Chendu, China, 20–22 August 2010; IEEE: Piscataway, NJ, USA, 2010; Volume 2, pp. 123–126.
13. Biglari, H.; Golmohammadi, M.; Hayati, S.; Hemmati, S. Vibration reduction of a flexible robot link using a frictional damper. *J. Vib. Control.* **2021**, *27*, 985–997. [[CrossRef](#)]
14. Faieghi, M.; Atashzar, S.F.; Sharma, M.; Tutunea-Fatan, O.R.; Eagleson, R.; Ferreira, L.M. Vibration analysis in robot-driven glenoid reaming procedure. In Proceedings of the 2020 IEEE/ASME International Conference on Advanced Intelligent Mechatronics (AIM), Boston, MA, USA, 6–9 July 2020; IEEE: Piscataway, NJ, USA, 2020; pp. 741–746.
15. Berninger, T.F.; Fuderer, S.; Rixen, D.J. Modal analysis of a 7 DoF sweet pepper harvesting robot. In Proceedings of the 37th IMAC, A Conference and Exposition on Structural Dynamics, Orlando, FL, USA, 28–31 January 2019; Springer: Cham, Switzerland, 2019; Volume 8, pp. 163–170.
16. Rafieian, F.; Liu, Z.; Hazel, B. Dynamic model and modal testing for vibration analysis of robotic grinding process with a 6DOF flexible-joint manipulator. In Proceedings of the 2009 International Conference on Mechatronics and Automation, Changchun, China, 9–12 August 2009; IEEE: Piscataway, NJ, USA; pp. 2793–2798.
17. Fuentes, A.T.; Kipfmueller, M.; Prieto, M.J. 6 DOF articulated-arm robot and mobile platform: Dynamic modelling as Multibody System and its validation via Experimental Modal Analysis. In Proceedings of the IOP Conference Series: Materials Science and Engineering, 4th International Conference on Mechanical Engineering Research (ICMER2017), Lumut, Malaysia, 1–2 August 2017; IOP Publishing: Bristol, UK, 2017; Volume 257, p. 012008.
18. Ariano, A.; Perna, V.; Senatore, A.; Scatigno, R.; Nicolò, F.; Fazioli, F.; Avallone, G.; Pesce, S.; Gagliano, A. Simulation and Experimental Validation of Novel Trajectory Planning Strategy to Reduce Vibrations and Improve Productivity of Robotic Manipulator. *Electronics* **2020**, *9*, 581. [[CrossRef](#)]
19. Min, F.; Wang, G.; Liu, N. Collision detection and identification on robot manipulators based on vibration analysis. *Sensors* **2019**, *19*, 1080. [[CrossRef](#)] [[PubMed](#)]
20. Bottin, M.; Cocuzza, S.; Comand, N.; Doria, A. Modeling and identification of an industrial robot with a selective modal approach. *Appl. Sci.* **2020**, *10*, 4619. [[CrossRef](#)]
21. Nguyen-Van, S.; Gwak, K.W.; Nguyen, D.H.; Lee, S.G.; Kang, B.H. A novel modified analytical method and finite element method for vibration analysis of cable-driven parallel robots. *J. Mech. Sci. Technol.* **2020**, *34*, 3575–3586. [[CrossRef](#)]
22. Ivanov, S.; Zudilova, T.; Ivanova, L.; Meleshkova, Z.; Voitiuk, T. Vibration Protection of the Robotic Arm from External Effects on the Base. In Proceedings of the 26th Conference of Open Innovations Association FRUCT, Yaroslavl, Russia, 20–24 April 2020; Volume 26, pp. 514–522, FRUCT Oy.
23. Zhang, Q.; Fotouhi, R.; Cote, J.; KhakPour, M. Lightweight long-reach 5-dof robot arm for farm application. In Proceedings of the International Design Engineering Technical Conferences and Computers and Information in Engineering Conference, Anaheim, CA, USA, 18–21 August 2019. DETC2019-98366.
24. Stolarski, T.; Nakasone, Y.; Yoshimoto, S. *Engineering Analysis with ANSYS Software*, 2nd ed.; Butterworth-Heinemann: Oxford, UK, 2018.